Ground-state characterization of Nb charge-phase Josephson qubits

H. Zangerle, J. Könemann, B. Mackrodt, R. Dolata, S. V. Lotkhov, S. A. Bogoslovsky, M. Götz, and A. B. Zorin
Physikalisch-Technische Bundesanstalt, Bundesallee 100, 38116 Braunschweig, Germany
(Received 9 February 2006; revised manuscript received 2 May 2006; published 28 June 2006)

We present investigations of Josephson charge-phase qubits of superconducting quantum interference device (SQUID) configuration, inductively coupled to a radio-frequency-driven tank circuit, enabling the readout of the states by measuring the Josephson inductance of the qubit. The circuits, including junctions with linear dimensions of 60 nm×60 nm and 80 nm×80 nm, are fabricated from Nb/AlO_x/Nb trilayer and allow the determination of relevant sample parameters at liquid helium temperature. The observed partial suppression of the circulating supercurrent in the qubit loop at 4.2 K is explained within the framework of a quantum-statistical model. We have probed the ground-state properties of qubit structures with different ratios of the Josephson coupling to Coulomb charging energy at 20 mK, demonstrating both the magnetic control of phase and the electrostatic control of charge of the qubit.

DOI: 10.1103/PhysRevB.73.224527 PACS number(s): 74.50.+r, 85.25.Cp, 73.40.Gk

I. INTRODUCTION

Superconducting structures with mesoscopic Josephson tunnel junctions can provide a basis for electronic devices operating on single Cooper pairs. Prominent examples are the superconducting quantum bit (qubit) circuits, which are regarded as promising elements for a scalable quantum computer.[1] The Josephson charge-phase qubit[2] is based on a Cooper-pair box[3] of superconducting quantum interference device (SQUID) configuration, i.e., a superconducting loop interrupted by two small-capacitance junctions with an island in between, which is capacitively coupled to a gate electrode (i.e., the Bloch transistor[4]). The charging energy E_C and the Josephson coupling energy E_J are typically of the same order, so the dimensionless parameter $\lambda = E_J/E_C$ is of the order of one. Moreover, our circuit comprises both the qubit and its readout.[5] The transistor can be operated as a box (qubit) whose distinct quantum states with energies $E_n, n = 0,1,2,\ldots$, are associated with different Bloch-bands of the system.[6] The eigenfunctions $|n,q\rangle$ are the Bloch wave functions of a particle in the periodic (Josephson) potential. Here, n is the band number and q the quasicharge governed by the gate voltage V_G, i.e., $q = C_G V_G$, where C_G is the gate capacitance (see, e.g., Ref. 7). The quantum states of the transistor also involve the phase coordinate φ set by the external magnetic flux Φ_{dc} applied to the SQUID loop. The variable φ behaves almost classically and is regarded as a parameter. Because of two control parameters (charge and phase), the eigenenergies $E_n(q,\varphi)$, the transition frequency $\nu_{10} = (E_1 - E_0)/h$, and—in the case of multiple qubits—the strength of mutual coupling can be varied in the wide range. The readout of our qubit can be performed similar as in the rf-SQUID-based impedance measurement technique pioneered by Rifkin and Deaver:[8] the qubit eigenstates can be distinguished by the Josephson inductance of the effective weak link, i.e., the transistor, included in the loop whose impedance is probed by small rf oscillations induced by an inductively coupled resonant tank circuit;[5,9] see the equivalent circuit in Fig. 1.

Recently, Born *et al.*[10] have confirmed the aforementioned readout conception in a spectroscopic experiment with an Al qubit. The authors demonstrated the detection of microwave-power-induced interband transitions by tracking the resonant response of the tank. However, because of the rather large ratio $\lambda = E_J/E_C \approx 30$, manipulation of the qubit state via its gate was in their experiment limited to a narrow ($\sim 5\%$) interval of values of the flux. In this paper, we present a comprehensive mapping of the ground state of Nb qubits operating in the charge-phase regime over a wide range of the parameters q and φ. This is done for the most illustrative case of the values of the parameter $\lambda \sim 1$. In this regime, the behavior of the system strongly depends on the value of λ. Moreover, the effect of thermal fluctuations is studied comparatively at 20 mK and 4.2 K for the same samples. These investigations strongly benefit from the advanced technology for the fabrication of submicron Josephson junctions based on Nb/AlO_x/Nb trilayers with a large superconducting energy gap Δ and a low subgap leakage current.[11] Applying this technology allows all inductive components of the circuitry shown in Fig. 1 to be integrated on one chip.

The material presented in this paper is organized as follows. In Sec. II, we briefly outline the considerations that motivated our choice of experimental parameters. In Sec. III, radio-frequency measurement results for niobium-based Bloch transistors will be presented and quantitatively analyzed. Especially, the fluctuation-induced partial suppression of the critical current through Bloch transistors will be dis-

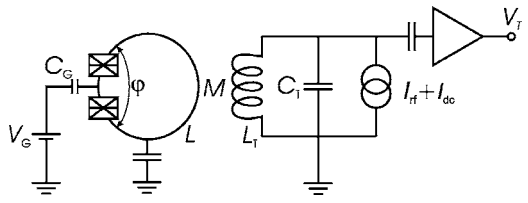

FIG. 1. Scheme of the experiment. The core element is a double Josephson junction (two crossed boxes) with a capacitive gate coupled to its island, i.e., the Bloch transistor, embedded in a macroscopic superconducting loop. The loop is inductively coupled to an rf-driven tank circuit connected to a cold preamplifier. The capacitance between the loop and the ground is assumed to be much larger than the total capacitance of the island.

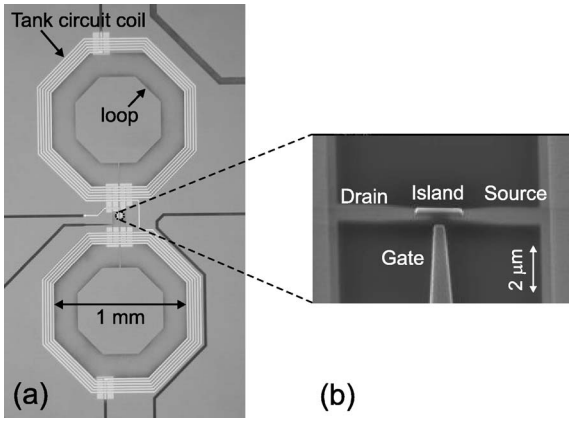

FIG. 2. (a) The image of the sample of the gradiometer configuration with the Bloch-transistor structure in the center. (b) The zoomed-in microphotograph of the transistor, which is located between two parallel wires terminated by the loops at both sides. Thus, the loops are connected in parallel, resulting in the total inductance L equal to one half of the inductance of each loop.

cussed within a quantum-statistical model. In Sec. IV the concluding remarks will be made.

II. DESIGN OF EXPERIMENT

A. Parameters of the samples

The operation of a charge-phase qubit based on the single charge phenomena thus requiring the charging energy $E_C = e^2/2C$ of the small island electrode ($C = C_{J1} + C_{J2} + C_G$ denotes the corresponding total capacitance, including the capacitances of the junctions $C_{J1,J2}$) to be large, compared to the thermal energy $k_B T$. In the case of our Nb technology, the parameter $E_C \approx 50-80$ μeV roughly corresponds to temperature ~ 1 K. The rather balanced situation with the target value $\lambda \sim 1$, i.e., the Josephson coupling energy of individual junctions $E_{J0} = (\Phi_0/2\pi) I_{c0} \approx 50-100$ μeV, where $\Phi_0 = h/2e \approx 2.07 \times 10^{-15}$ Wb is the magnetic flux quantum, corresponds to nominal critical currents of the individual junctions I_{c0} of several tens of nanoamperes.[12]

The Bloch transistor is included in a double superconducting loop of octagon shape with an outer dimension of 1.0 mm (see Fig. 2). Such a gradiometer design improves the stability against homogeneous magnetic field noise. The total inductance value of such a loop $L \approx 0.7$ nH was estimated using Mohan's formula.[13] This value is sufficiently small in the sense that, first, the corresponding magnetic energy is rather large, i.e., $E_M = \Phi_0^2/2L \approx 20$ meV and, second, the dimensionless screening parameter, i.e., $\beta_L \equiv 2\pi L I_{c0}/\Phi_0 \ll 1$, is small. The former relation ensures the suppression of flux fluctuations and fixes the phase φ across the transistor.[14] The latter one ensures the required nonhysteretic operation regime in the case of a single-junction SQUID circuit,[8,15] as well as of the realistic qubit circuit having finite asymmetry in the critical currents of individual junctions.[9] Moreover, the total inductance of the closed-loop circuit is determined mostly by the transistor Josephson inductance. This inductance is directly related to the local curvature of the surface $E_n(q, \varphi)$ taken for fixed q,[9] i.e.,

$$L_J(n, q, \varphi) = \left(\frac{\Phi_0}{2\pi}\right)^2 \left[\frac{\partial^2 E_n(q, \varphi)}{\partial \varphi^2}\right]^{-1}. \quad (1)$$

In our measurements of the circuit in the ground state, the band index $n=0$; thus we introduce the notation $L_J(0, q, \varphi) \equiv L_J(q, \varphi)$.

The loop is coupled through the mutual inductance M to the coil of a resonant tank circuit formed by the double octagon-shaped spiral inductor with total inductance $L_T = 0.15-0.2$ μH [see Fig. 2(a)] and the capacitance of the coaxial cable connecting the tank to the preamplifier. The bare resonance frequency of such a tank circuit with quality factor $Q \approx 250$ is $f_0 \approx 70$ MHz. Because of the coupling to the qubit, the effective inductance of the circuit is changed,[15]

$$L_{\text{eff}} = L_T - M^2 L_J^{-1}(q, \varphi), \quad (2)$$

in a gate-charge and phase-specific way. The resulting shift Δf of the resonant frequency, is[9]

$$\frac{\Delta f}{f_0} = -\frac{1}{2} k^2 \beta_L \frac{\Phi_0/2\pi I_c}{L_J(q, \varphi)}. \quad (3)$$

Here, $k = M/\sqrt{L L_T} < 1$ denotes the coupling coefficient, which is determined by the arrangement of the inductively coupled conductors. The integrated on-chip design of our qubit allows close mutual arrangement of the loop and the coil and, therefore, rather large values of k. The tank circuit is driven by a combined current signal, consisting of a dc part fixing the working point and an rf component I_{rf} at the frequency f close to f_0.

The cold preamplifier is based on an AGILENT ATF-10136 GaAs field-effect transistor, which has the main task of matching of the impedance of the tank circuit and the cabling. The output of the preamplifier is connected by the coaxial cable to the room-temperature amplifier. Although our two-stage amplifier can operate in the wide-frequency range, it works most stable in the range between 60 and 90 MHz with a frequency-independent overall gain of 26 dB. Its noise temperature is evaluated to be about 1.2 K. The amplified rf voltage across the tank is fed to a lock-in amplifier measuring both the amplitude V_T and the phase shift α relative to the reference rf signal.

B. Precharacterization of Bloch transistors

Embedding the Bloch transistors in a superconducting loop, unfortunately, renders its precharacterization in a simple dc configuration impossible. To get nevertheless an estimate of the relevant parameters, i.e., the Josephson coupling energy E_{J0} and the charging energy E_C, we characterized the similar stand-alone Bloch transistor structures fabricated from the same wafer, hence, made from the same $Nb/AlO_x/Nb$ trilayer and having the same dimensions. From I-V measurements at 4.2 K [shown in Fig. 3(a)], we extract the sum asymptotic resistance R_Σ and the gap voltage V_{Gap}. Resistance R_Σ is assumed to equal twice the normal state resistance $R_N \approx 33.5$ kΩ of one from two nominally identical junctions while the superconductor energy gap $\Delta = eV_{\text{Gap}}/4 \approx 1.04$ meV. Inserting these values into the Ambegaokar-Baratoff relation $R_N I_{c0} \approx (\pi/2)\Delta/e$,[16] we estimate the critical

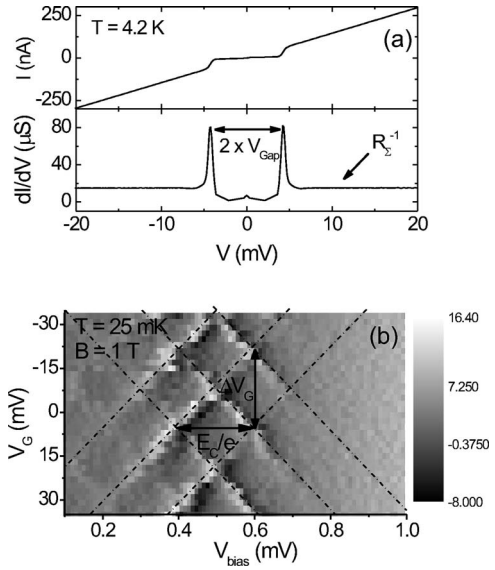

FIG. 3. (a) Typical dc I-V curve of the stand-alone test transistor from wafer B at 4.2 K. The superconducting gap-voltage in this sample is $V_{\mathrm{Gap}}=4.17$ mV and the normal-state resistance $R_{\Sigma}=67$ kΩ of the series double-junction (transistor). (b) Contour-plot of the differential conductance dI/dV in μS of an isolated test transistor of wafer B as a function of gate voltage and bias voltage measured at 25 mK.

current I_{c0} and finally, E_{J0} the Josephson coupling energy of one junction as listed in Table I. Note that I_{c0} values of 25 nA (wafer A) respectively 45 nA (wafer B) differ almost by a factor of 2. The radio-frequency measurements performed at 4.2 K with the single junctions inserted instead of the transistors in the similar loops (see Fig. 1), i.e., the rf-SQUID configuration, gave almost similar values for I_{c0}.

The values of E_{C} were derived from the gate and bias voltage dependencies of the current of the stand-alone transistors at 20 mK and perpendicular magnetic field of up to 2 T. This magnetic field partially suppresses the superconductivity of the Nb electrodes and enhances the single-electron tunneling at small voltage bias.[17] For the bias below the gap voltage, we found the characteristic diamondlike pattern resulting from Josephson quasiparticle cycles;[18] the bias

TABLE I. Parameter overview for the experiments with the Bloch transistor samples T1 (from wafer A) and T2 (from wafer B).

	T1 (60 nm × 60 nm)	T2 (80 nm × 80 nm)
E_{J0} (μeV)	50	95
E_{C} (μeV)	80	45
L (nH)	0.7	0.7
L_{T} (μH)	0.20	0.15
M (nH)	4.6	3.8
k	0.42	0.39
I_{c} (nA)	3.9	17
β_{L}	0.008	0.036
f_0 (MHz)	68.80	76.18
Q	250	235

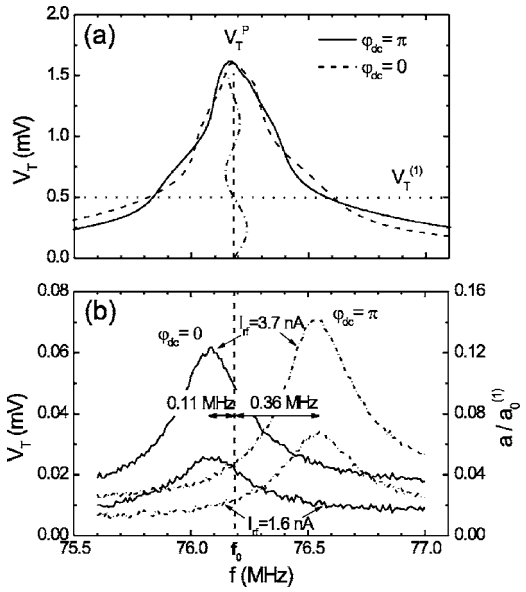

FIG. 4. (a) Typical resonance curves for sample T2 (fabricated from wafer A) at 20 mK. Shown is the detected tank-circuit voltage as a function of the applied frequency of the rf excitation for a driving current of $I_{\mathrm{rf}}\approx 89$ nA. The dashed-dotted line shows the amplitude-dependency $f(a)$ of the resonance-frequency for an assumed harmonic phase-dependence, as described by Eq. (4). (b) Typical resonance curves of sample T2 for a low excitation power, i.e., driving-currents $I_{\mathrm{rf}}\approx 1.6$ nA and $I_{\mathrm{rf}}\approx 3.7$ nA. The asymmetric shifts of the two resonance curves at extreme values of φ_{dc} with respect to the tank circuit resonance frequency f_0 results from the pronounced nonharmonic current-phase relation in sample T2, compare Fig. 6(b).

voltage period provides an estimate of the charging energy [see Fig. 3(b) and Table I], while the gate voltage period $\Delta V_{\mathrm{G}}\approx 28$ mV gives the value of the gate capacitance, $C_{\mathrm{G}}=e/\Delta V_{\mathrm{G}}\approx 6$ aF.

III. RADIO-FREQUENCY MEASUREMENTS

A. Resonance curves

First, the resonance measurements of the Bloch transistors were performed in order to calibrate the rf oscillation amplitude of the phase, $\varphi(t)=\varphi_{\mathrm{dc}}+a\sin(2\pi ft)$, with a being proportional to the amplitude of the rf-flux oscillations in the loop, $\Phi_a=a\Phi_0/2\pi$. In these measurements we applied an rf driving current I_{rf} via a cold divider from the generator to the tank circuit. An external dc bias current (see Fig. 1) was added with the aid of a bias tee. The resonance curves V_{T}-f for a moderate pumping amplitude are shown in Fig. 4(a). The curves exhibit characteristic "nodes" typical of rf SQUIDs,[19] where, at certain pumping levels, the sensitivity of the tank oscillation amplitude against the dc bias, i.e., the stationary Josephson phase difference φ_{dc}, disappears. Assuming a sinusoidal current-phase relation (CPR), these "nodes" are related to the amplitude-dependent resonant frequency for fixed φ_{dc} given by the formula:[20]

$$f(a)=f_0\{1+k^2\beta_{\mathrm{L}}[J_1(a)/a]\cos\varphi_{\mathrm{dc}}\} \tag{4}$$

with $J_1(a)$ denoting the first-order Bessel-function. If a equals one of the positive zeros $a_0^{(i)}$ $(i=1,2,)$ of function J_1,

the resonant frequency is no longer dependent on φ_{dc} or on the dc bias current. The amplitude $V_T^{(1)}$ for the first node can be assigned to the respective value $a_0^{(1)}$, thus providing calibration according to $a=3.83V_T^p/V_T^{(1)}$, where $V_T^p=\max(V_T)$. From the value of V_T^p, one can estimate the amplitude of the driving-current I_{rf} as $I_{rf}=YV_T^p$, where the impedance of the circuit at resonance is $1/Y=2\pi f_0 L_T Q \approx 18\ k\Omega$.

The good agreement between the calculated $f(a)$-dependence (dash-dotted line in Fig. 4(a)) and the position of the nodes illustrates that the transistor sample investigated behaves for rather large amplitudes approximately as an element with harmonic CPR. In other words, the contribution of higher harmonics in the CPR to the resulting resonance frequency $f(a)$ is small.

For the small pumping levels, the resonance curve is shifted as a whole when changing the dc bias current, see Fig. 4(b). In contrast to the situation for the large amplitude of oscillations, the nonharmonic shape of the CPR plays a crucial role here as expressed by Eq. (1), relating the local curvature of the band with the Josephson inductance. The frequency shift determined for the two opposite values of the external dc magnetic flux applied to the loop is no longer symmetric relative to the tank-circuit frequency since the reverse inductance $L_J^{-1}(q,\varphi)$ producing this shift [see Eq. (3)] is not exactly proportional to $\cos\varphi$ here. This asymmetric splitting appears so clear in our experiment because of the rather large value of the product $k^2Q\beta_L \approx 1.6$ for sample T2 (cf. experiments on rf-SQUIDs with large values of this product in Ref. 21). The minimum rf excitation, which allows us to work with a sufficiently high signal-to-noise ratio in our measurements, corresponds to values $a \approx 0.1a_0^{(1)}$.

For a sufficiently small value of a, the phase angle α between the driving signal I_{rf} and the voltage oscillations is given by

$$\tan\alpha = 2Q\left(\frac{\Delta f}{f_0-\xi}\right), \tag{5}$$

with the resonance frequency detuning Δf resulting from the transistor's Josephson inductance Eq. (3) and the relative shift $\xi=(f\text{-}f_0)/f_0$ of the operation frequency f. The measurement of this angle for different values of the dc flux and gate charge at a sufficiently low temperature allows the curvature of the qubit ground-state surface to be mapped.

B. Radio-frequency measurements at 4.2 K

As long as our samples are fabricated from Nb films having a critical temperature of about 9 K, they preserve the Josephson properties and can be measured at a temperature of $T=4.2$ K. Earlier, the rf measurements of transistors, which comprise somewhat larger Nb junctions (with dimensions down to 300 nm $\times$ 300 nm) and are included in low-inductance loops were successfully carried out at 4.2 K by Il'ichev *et al.*[22] These samples showed a clear dependence of the phase angle on the applied dc flux and allowed the critical current of the junctions to be evaluated ($\sim$55 nA). Because of the large capacitance of the island in these samples, the charging energy was small (about 4 μeV, i.e., 50 mK)

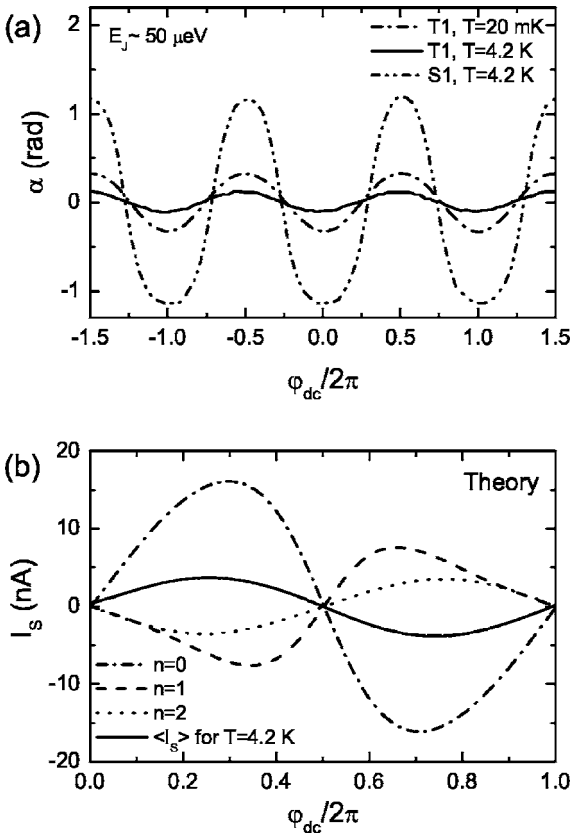

FIG. 5. (a) Phase-shift α as a function of the phase ($\varphi_{dc} \propto \Phi_{dc}$) for a single-junction (dashes-double-dotted line) of wafer A at 4.2 K and for the double-junction sample $T1$ of wafer A at 20 mK (dashed-dotted line) and 4.2 K (solid line). The nominal value of the Josephson energy of each junction of wafer A is about 50 μeV. (b) Current-phase relations for the ground band (dashed-dotted line), the first (dashed line), and second band (dotted line) of the Bloch-transistor calculated for $E_{J0}=100$ μeV, $E_C=45$ μeV, and $q=0.5$. The thick solid line indicates the observable value of the supercurrent $I_S(\varphi,q)$ derived from Eq. (8).

and the values of parameter λ were rather large (>30); thus, these transistors behaved classically at an operation temperature of 4.2 K, i.e., like two classical Josephson junctions connected in series. Remarkably, our qubit samples with significant charging energy (i.e., $\lambda \sim 1$), and thus a large Coulomb suppression of I_c,[7] also exhibited a clear dependence of α on the dc flux at this temperature. This means, that our experiment allowed the monitoring at 4.2 K of very small effective critical currents of the order of 7 nA (cf. 55 nA measured in Ref. 22).

Figure 5(a) shows the periodic dependencies α-φ_{dc} measured in the qubit sample T1 (fabricated from wafer A) at 4.2 K (solid line) and 20 mK (dashed-dotted line). For comparison, the corresponding curve (measured at 4.2 K) for the similar single Josephson junction included in the identical rf circuit is shown by a dashed-double-dotted line. This plot demonstrates first the reduction of the critical current of the transistor in the ground state at $T=20$ mK ($k_BT \ll E_J, E_C$) in comparison to a single junction. This is due to the charging effect of the island (see, for example, the experiments[23,24]). Second, one can see a further reduction of the critical current

observed at the elevated temperature of 4.2 K.

Such behavior can be explained by a simple model, that takes the mixed Bloch states at values of thermal energy k_BT into account that are comparable to the interband energies. In this case the observable supercurrent $\langle \hat{I}_S \rangle$ is found as the quantum-statistical averaging over the canonical ensemble,

$$I_S(\varphi,q) = \langle \hat{I}_S \rangle = \frac{\mathrm{Tr}(\hat{I}_S e^{\hat{H}/k_BT})}{\mathrm{Tr}(e^{\hat{H}/k_BT})}, \tag{6}$$

where $\hat{H}$ denotes the Hamiltonian of the total system including the electromagnetic environment in the thermal equilibrium at a temperature T. In view of the small gate capacitance ($C_G \ll e^2/2k_BT$) and the small loop inductance ($L < (\Phi_0/2\pi)^2/k_BT$), the variables φ and q can be regarded as classical parameters. The full expression for the supercurrent operator $\hat{I}_S$ was derived in Ref. 9. The diagonal matrix elements contributing to the expectation value entering in Eq. (6) are, therefore, equal to

$$\langle n|\hat{I}_S|n\rangle = \frac{2\pi}{\Phi_0}\frac{E_{J1}E_{J2}}{E_J(\varphi)} \sin\varphi \langle n|\cos\chi|n\rangle, \tag{7}$$

where the effective Josephson coupling energy of the transistor is given by $E_J(\varphi) = (E_{J1}^2 + E_{J2}^2 + 2E_{J1}E_{J2}\cos\varphi)^{1/2}$ and χ is the operator of the transistor island's phase (conjugate to the operator of the island's charge). Note that the value $|\langle n|\cos\chi|n\rangle| < 1$ (see the plots of this matrix element for $n=0$ in Ref. 7) also depends on the phase φ, because φ determines the ratio $\lambda = E_J(\varphi)/E_C$.

Note that, due to the different signs of the term $\langle n|\cos\chi|n\rangle$, the supercurrent in the different Bloch bands $\langle n|\hat{I}_S|n\rangle$, $n=0,1,2,\ldots$. has usually inverted the phase dependencies (see the calculated curves in Fig. 5(b) as well as Fig. 3 in Ref. 5). These antiphase terms contribute with the corresponding Boltzmann's factors to the observable value Eq. (6). Finally, the supercurrent value to be detected in the 4.2 K measurement is equal to

$$I_S(\varphi,q) = \left(\frac{2\pi}{\Phi_0}\right) E_{J1}E_{J2} \sin\frac{\varphi}{E_J(\varphi)} \sum_{n=0}^{N}\sum_{m=0}^{1} \langle n|\cos\chi|n\rangle \times e^{-E_n(q+me,\varphi)/k_BT} \sum_{n=0}^{N}\sum_{m=0}^{1} e^{-E_n(q+me,\varphi)/k_BT}. \tag{8}$$

Here, E_n is the eigenenergy of the system taken at the corresponding values of q and φ. The summation over m takes into account both even and odd configurations of charge on the island. In the odd states ($m=1$) we omit the contribution of $\Delta > k_BT$ to the energy E_n related to an unpaired electron. Thus, in our model we assume the existence of electron states inside the energy gap in the spectrum of the island. Both of these configurations are realized due to the unavoidable single electron tunneling at the elevated temperature. An analysis of Eq. (8) shows that, taking into account the three lowest energy bands (i.e., choosing $N=2$), is sufficient for an adequate description of our experiments with the given sample parameters and temperatures up to $T=4.2$ K. Then, higher bands ($n>2$) are sparsely populated and do not essentially contribute to I_S. As a tendency, the dependence of $I_S(\varphi,q)$ on the gate charge q practically vanishes as soon as higher bands get involved. The phase dependence becomes almost harmonic.

TABLE II. Theoretical and experimental values of the critical currents of two Bloch transistor samples at a sufficiently low temperature of 20 mK and at 4.2 K. For the $I_c^{(th)}$ calculation based on the parameters E_{J0} and E_C listed in Table I, $E_{J0}=E_{J1}=E_{J2}$ is assumed as justified by the weak influence of the imbalance parameter $b=(E_{J1}-E_{J2})/(E_{J1}+E_{J2})$ found in the simulations.

	T1	T2
$I_c^{(th)}$ at $T=20$ mK	4.5 nA	16 nA
$I_c^{(m)}$ at $T=20$ mK	3.9 nA	17 nA
$I_c^{(th)}$ at $T=4.2$ K	0.9 nA	4.3 nA
$I_c^{(m)}$ at $T=4.2$ K	0.6 nA	3.0 nA

In Table II, we compare the critical-current values calculated according to our model, $I_c^{(th)}$, with those extracted from the measurements, $I_c^{(m)}$, for both our transistor samples at 20 mK and 4.2 K. From the experimental data, we obtained the critical currents according to the relation

$$I_c^{(m)} = \frac{\Phi_0}{2\pi}\frac{\tan(\delta\alpha/2)a}{k^2QLJ_1(a)}, \tag{9}$$

following from Eqs. (3) and (5). Here we introduce the value $\delta\alpha = \max_{\{\Phi_{dc}\}}\alpha - \min_{\{\Phi_{dc}\}}\alpha$. For both temperatures considered here, we find that the theoretical and experimental critical currents are in good agreement. Moreover, the fact that $I_c^{(th)}$ does not differ for zero temperature and 20 mK, indicates that measurements at the base temperature of the dilution refrigerator explore, indeed the ground state, since in the $1e$-periodic regime, i.e., for the gate charge between $-e/2$ and $e/2$ (mod 2) the contribution of higher bands due to nonequilibrium effects is negligible because of the large gap Δ in Nb and the large energy band spacing in this gate range.

C. Mapping of the ground state

Figure 6 presents the phase dependence as a function of both external dc-flux (corresponding to the Josephson phase φ) and the gate-voltage V_G proportional to the quasicharge q for the samples T1 and T2. A nearly sinusoidal dependence of the phase α on φ_{dc} is to be seen that is modulated periodically by the applied gate voltage V_G.

A closer look at Fig. 6 reveals that the amplitude of the oscillations of α and, therefore, the critical current is smaller in T1 than in T2, as expected from the Ambegaokar-Baratoff values of E_J and also because of the smaller λ ratio, due to the charging effects. The nominal values E_{J0} differ by less than a factor of 2, whereas the critical currents differ by more than a factor of 4. Related to that, the dc-bias dependence of α is closer to the sinusoidal one for sample T1 having the smaller value of $\lambda = 0.7$.[25] In contrast to this, the corresponding dependence for sample T2 (see Fig. 6(b)) having larger

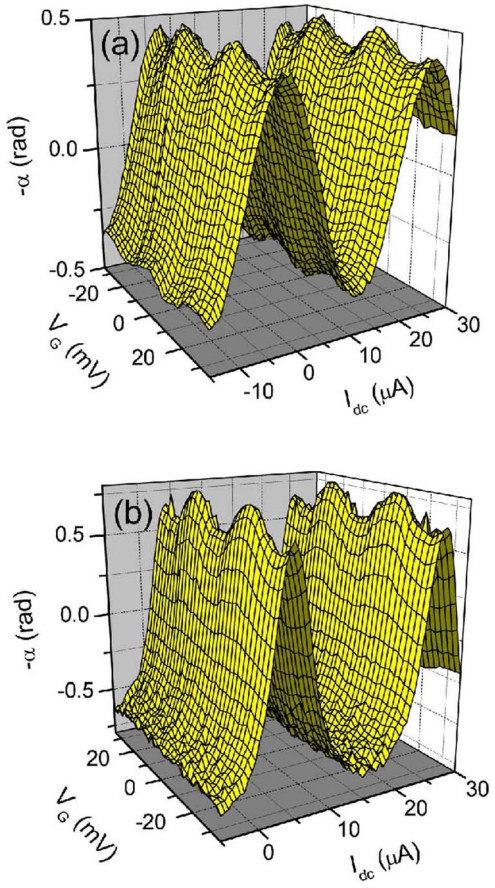

FIG. 6. (Color online) Phase-shift α as a function of the applied dc-flux ($\propto I_{dc}$) and gate voltage V_G at $T=20$ mK for samples (a) T1 and (b) T2.

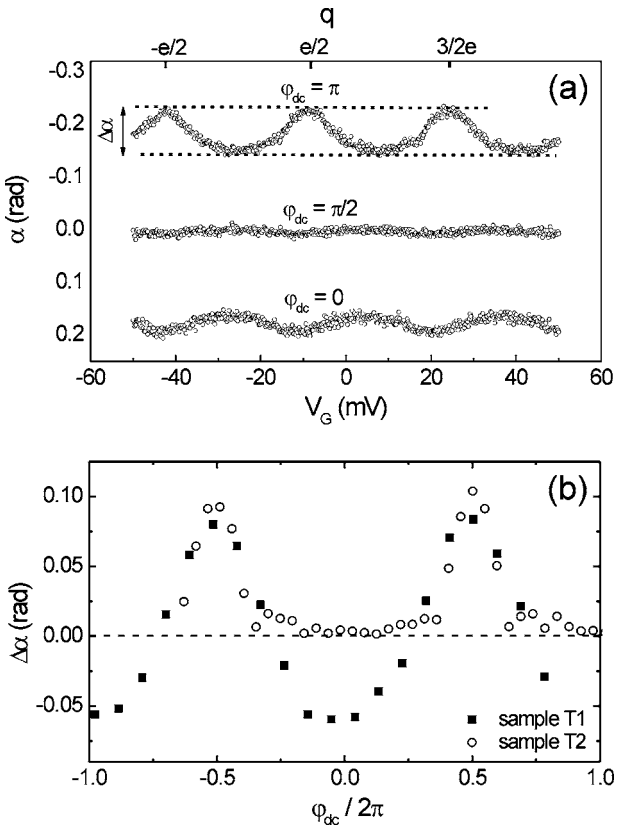

FIG. 7. (a) Gate modulation curves $\alpha(V_G)$ of T1 for three different values of the applied magnetic flux. The curves are shifted for clarity. (b) Dependence of the peak-to-peak value $\Delta\alpha$ of the gate modulation as a function of the external magnetic flux for T1 and T2. The negative values of $\Delta\alpha$ have the meaning of the reverse phase dependencies in plot (a).

$\lambda \approx 1.9$ is clearly nonharmonic resulting in an asymmetric shift of the resonance curves in Fig. 4(b).

Gate-modulation curves of sample T1 (low λ-ratio) for different values φ_{dc} are displayed in Fig. 7(a). We find a periodic gate-modulation curve with a modulation depth $|\Delta\alpha|$ of 0.05 rad for $\varphi_{dc}=0$ and of 0.09 rad for $\varphi_{dc}=\pi$, whereas for $\varphi_{dc}=\pi/2$, the gate charge sensitivity disappears almost completely. The gate-dependence period ΔV_G is roughly 29 mV for both samples and complies with the value found for the stand-alone test transistor shown in Fig. 3(b). In contrast to our recent measurements on Al-qubit samples with similar layout,[26] the gate oscillations are $1e$-periodic. Since the periodicity of the Nb samples does not change when applying a magnetic field of 2 T that is sufficient to cause intensive quasiparticle tunneling,[17] we think that the $1e$-periodicity originates from the presence of presumably few unpaired quasiparticles[27] on the transistor island changing its parity. Because of the large Δ of Nb the presence of nonequilibrium quasiparticles[23,28] is less likely.

One should note that the gate modulation appears for sample T1 over the whole range of phase φ_{dc}, hence allowing efficient qubit control over the whole flux bias range. On the other hand, for sample T2 ($\lambda=1.9$), the modulation depth is nonzero only in the vicinity of the point $\varphi_{dc}=\pi$ (cf. Ref. 10, where this range was notably smaller) and almost zero for the rest of the flux-bias range; see Fig. 7(b).

The surface plots of the phase shift presented in Fig. 6 should reflect the dependence of the local curvature of the ground-state energy on q and φ [see Eq. (1)]. However, because of the finite amplitude of the oscillations, $a \sim 0.1 a_0^{(1)}$, of phase φ these surfaces yield the values of curvature averaged over the finite interval. Such averaging of the reverse Josephson inductance is described by the integral

$$L_J^{-1}(q,\varphi) \to \frac{1}{\pi}\int_{-1}^{1} L_J^{-1}(q,\varphi + ax)\frac{dx}{\sqrt{1-x^2}}. \qquad (10)$$

This expression makes it possible to compare the obtained experimental data to the corresponding dependencies following from the theory, taking into account the local curvature of the ground-state energy and the finite amplitude of the phase oscillations. By inserting the known parameters E_{J0}, E_C, Q, Δf, k, and a into Eqs. (3), (5), and (10), we calculate the dc bias modulation curves for arbitrary charge on the transistor gate. The curves for $q=0$ and $q=0.5e$ are shown in Fig. 8. These curves, which are based on input data partly deduced from the dc measurements described in Sec. II, agree well with the primary data from the rf experiments.

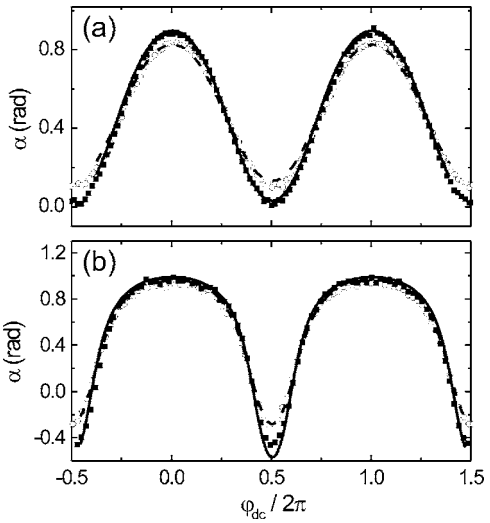

FIG. 8. Experimental phase shift for samples (a) T1 and (b) T2 for two different values of the gate charge $q=0$ (open circles) and $q=0.5e$ (closed squares). The calculated dependencies are represented by solid lines ($q=0.5e$) and dashed lines ($q=0$), respectively.

IV. CONCLUSION

The radio-frequency impedance measurements of the charge-phase qubit samples with balanced Josephson coupling to Coulomb charging energy ratio λ clearly demonstrated the dependence of the curvature of the ground-state energy on the control charge and phase in a wide range. The shape of the Josephson inductance surface of the transistor is well described by the Bloch band theory.

An advantage of our Nb technology is that we were able to characterize our qubit system at a temperature of $T=4.2$ K. In our investigation, we found that the Josephson critical current of the tunnel junctions forming the qubit is scaled with their size, almost approaching the nominal Ambegaokar-Baratoff value. The availability of sub-0.1 μm niobium-based Josephson junctions was extremely helpful as it offered the valuable possibility of studying the influence of thermal fluctuations in an extended temperature range without increasing the cryogenic efforts. The experimental results obtained at the large temperature can be interpreted within a simple quantum-statistical model of the Bloch transistor.

Although the measured qubit samples T1 and T2 had a charging energy E_C of the island (equal to 80 and 45 μeV, respectively) much smaller than the value of the Nb energy gap, >1 meV, this relation did not ensure the desired suppression of the quasiparticle tunneling. As result, instead of the $2e$-, the $1e$-periodic dependence of the qubit Josephson inductance on the gate charge was observed. Such behaviour of the stand-alone Nb transistor samples was also observed in earlier measurements performed in dc configuration; see Ref. 11, and references therein. As was suggested in Ref. 11, this behavior is most probably due to possible intragap energy states formed in $Nb/AlO_x/Nb$ tunnel barriers. Therefore, further improvement of the Nb technology of fabrication is required. On the other hand, the given Nb qubit samples can still operate in the "magic" points corresponding to the value of the control charge $q=0$. The question as to the rate of the quasiparticle tunneling in the excited state, presenting the most critical mechanism of the qubit relaxation,[9] deserves a special study.

ACKNOWLEDGMENTS

We wish to thank H.-P. Duda and R. Harke for valuable technical assistance and I. Novikov for useful comments. As well, we would like to acknowledge Th. Weimann and P. Hinze for their support with the electron-beam writer and B. Egeling and R. Wendisch for their support in the PECVD and CMP processes. This work was supported by the European Union (projects SQUBIT-2 and EuroSQIP).

[1] Y. Makhlin, G. Schön and A. Shnirman, Rev. Mod. Phys. **73**, 357 (2001).
[2] D. Vion, A. Aassime, A. Cottet, P. Joyez, H. Pothier, C. Urbina, D. Esteve, and M. H. Devoret, Science **296**, 886 (2002).
[3] V. Bouchiat, D. Vion, P. Joyez, D. Esteve, and M. Devoret, Phys. Scr., T **T76**, 165 (1998).
[4] D. V. Averin and K. K. Likharev, in *Mesoscopic Phenomena in Solids*, edited by B. L. Altshuler, P. A. Lee, and R. A. Webb (Elsevier, Amsterdam, 1991), p. 1753.
[5] A. B. Zorin, Physica C **368**, 284 (2002).
[6] K. K. Likharev and A. B. Zorin, J. Low Temp. Phys. **59**, 697 (1985); D. V. Averin, A. B. Zorin, and K. K. Likharev, Sov. Phys. JETP **61** (2), 407 (1985).
[7] A. B. Zorin, Phys. Rev. Lett. **76**, 4408 (1996).
[8] R. Rifkin and B. S. Deaver, Jr., Phys. Rev. B **13**, 3894 (1976).
[9] A. B. Zorin, JETP **98**, 1250 (2004).
[10] D. Born, V. I. Shnyrkov, W. Krech, Th. Wagner, E. Il'ichev, M. Grajcar, U. Hübner, and H.-G. Meyer, Phys. Rev. B **70**, 180501(R) (2004).
[11] R. Dolata, H. Scherer, A. B. Zorin, and J. Niemeyer, J. Appl. Phys. **97**, 054501 (2005).
[12] For the parameter range discussed here, the qubit transition frequency is of the order of 10 GHz in the optimum "magic" points of operation (Refs. 2 and 9), which is technically still convenient from the point of view of driving the qubit by microwave pulses.
[13] S. S. Mohan, M. del Mar Hershenson, S. P. Boyd, and T. H. Lee, IEEE J. Solid-State Circuits **34**, 1419 (1999).
[14] V. A. Khlus and I. O. Kulik, Sov. Phys. Tech. Phys. **20**, 283 (1975).
[15] P. K. Hansma, J. Appl. Phys. **44**, 4191 (1973).
[16] V. Ambegaokar and A. Baratoff, Phys. Rev. Lett. **10**, 486 (1963).
[17] A. B. Pavolotsky, T. Weimann, H. Scherer, V. A. Krupenin, J. Niemeyer and A. B. Zorin, J. Vac. Sci. Technol. B **17**, 230 (1999).
[18] M. T. Tuominen, J. M. Hergenrother, T. S. Tighe, and M. Tinkham, IEEE Trans. Appl. Supercond. **3**, 1972 (1993).
[19] V. I. Shnyrkov, V. A. Khlus, and G. M. Tsoi, J. Low Temp. Phys. **39**, 477 (1980).

[20] K. K. Likharev, *Dynamics of Josephson Junctions and Circuits* (Gordon and Breach, New York, 1986), Chap 14.
[21] I. M. Dmitrenko, G. M. Tsoi, V. I. Shnyrkov, and V. V. Kartsovnik, J. Low Temp. Phys. **49**, 417 (1982).
[22] E. Il'ichev, V. Zakosarenko, L. Fritzsch, R. Stolz, H. E. Hoenig, H.-G. Meyer, M. Götz, A. B. Zorin, V. V. Khanin, A. B. Pavolotsky, and J. Niemeyer, Rev. Sci. Instrum. **72**, 1882 (2001).
[23] P. Joyez, P. Lafarge, A. Filipe, D. Esteve, and M. H. Devoret, Phys. Rev. Lett. **72**, 2458 (1994).
[24] T. M. Eiles and J. M. Martinis, Phys. Rev. B **50**, 627(R) (1994).
[25] A. B. Zorin, IEEE Trans. Instrum. Meas. **46**, 299 (1997).
[26] J. Könemann, H. Zangerle, S. V. Lotkhov, B. Mackrodt, R. Dolata, A. B. Zorin, and J. Niemeyer (unpublished).
[27] M. T. Tuominen, J. M. Hergenrother, T. S. Tighe, and M. Tinkham, Phys. Rev. Lett. **69**, 1997 (1992).
[28] J. Aumentado, M. W. Keller, J. M. Martinis, and M. H. Devoret, Phys. Rev. Lett. **92**, 066802 (2004).